Hydrol. Earth Syst. Sci. Discuss., 11, 11987–12025, 2014
www.hydrol-earth-syst-sci-discuss.net/11/11987/2014/
doi:10.5194/hessd-11-11987-2014

Hydrology and Earth System Sciences
Open Access
Discussions

Spatial sensitivity analysis of snow cover data in a distributed rainfall–runoff model

T. Berezowski[1,2], **J. Nossent**[2], **J. Chormański**[1], **and O. Batelaan**[2,3]

[1]Department of Hydraulic Structures, Warsaw University of Life Sciences, Nowoursynowska 166, 02-787 Warsaw, Poland
[2]Department of Hydrology and Hydraulic Engineering, Vrije Universiteit Brussel, Pleinlaan 2, 1050 Brussels, Belgium
[3]School of the Environment, Flinders University, G.P.O. Box 2100, Adelaide, SA 5001, Australia

Received: 17 September 2014 – Accepted: 13 October 2014 – Published: 30 October 2014

Correspondence to: T. Berezowski (t.berezowski@levis.sggw.pl)

Published by Copernicus Publications on behalf of the European Geosciences Union.

Abstract

As the availability of spatially distributed data sets for distributed rainfall–runoff modelling is strongly growing, more attention should be paid to the influence of the quality of the data on the calibration. While a lot of progress has been made on using distributed data in simulations of hydrological models, sensitivity of spatial data with respect to model results is not well understood. In this paper we develop a spatial sensitivity analysis (SA) method for snow cover fraction input data (SCF) for a distributed rainfall–runoff model to investigate if the model is differently subjected to SCF uncertainty in different zones of the model. The analysis was focused on the relation between the SCF sensitivity and the physical, spatial parameters and processes of a distributed rainfall–runoff model. The methodology is tested for the Biebrza River catchment, Poland for which a distributed WetSpa model is setup to simulate two years of daily runoff. The SA uses the Latin-Hypercube One-factor-At-a-Time (LH-OAT) algorithm, which uses different response functions for each 4 km × 4 km snow zone. The results show that the spatial patterns of sensitivity can be easily interpreted by co-occurrence of different environmental factors such as: geomorphology, soil texture, land-use, precipitation and temperature. Moreover, the spatial pattern of sensitivity under different response functions is related to different spatial parameters and physical processes. The results clearly show that the LH-OAT algorithm is suitable for the spatial sensitivity analysis approach and that the SCF is spatially sensitive in the WetSpa model.

1 Introduction

Distributed hydrological models are developed to improve the simulation and analysis of physically based spatially distributed hydrological processes. While more spatially distributed parameters and input data are becoming available for modelling, most attention is paid to the influence of the data on the quality of the calibration and to the capacity of models to reproduce measured output time series. Several researchers

HESSD
11, 11987–12025, 2014

focussed on the effect of using distributed precipitation data in hydrological models. Obled et al. (1994) showed with a semi-distributed TOPMODEL (Beven et al., 1995) application that although the number of stations used to generate a rainfall field appeared to have an important impact on discharge simulation, the response of the model to changes in the rainfall field was marginal. Schuurmans and Bierkens (2007) used the fully-distributed SIMGRO (Querner, 1997) model to analyse the effect of rainfall fields generated on basis of rain gauge and radar data on discharge, soil moisture and groundwater heads. In their study, the distributed data outperformed lumped data in the simulation results. A similar study was conducted by Fu et al. (2011) who used the MIKE SHE model (Abbott et al., 1986). However, in this case a clear effect of rainfall distribution was visible only on groundwater head and recharge. In summary, the advantage of spatially distributed precipitation over lumped data may vary, depending on the model and the study area used. These studies could be more easily compared if a universal approach to quantify the sensitivity of a model to spatially distributed input data or parameters would be available. Such a methodology should allow to quantify in which zones of a study area the sensitivity of spatially distributed data with respect to the output is higher or lower and point to the causes for these differences.

An interesting stochastic uncertainty approach for spatial rainfall fields in the dynamic TOPMODEL (Beven and Freer, 2001)was presented by Younger et al. (2009). The results were obtained by dividing a catchment into homogeneous zones in which the precipitation was randomly perturbed by large factors. This study, however, focusses only on uncertainty and does not quantify spatial sources of uncertainty i.e. spatial sensitivity.

Stisen et al. (2011) investigated if using spatially distributed surface temperature data in an objective function can provide robust calibration and evaluation of the MIKE SHE model compared to lumped simulation. The study used a spatial perturbation of parameters by random factors between 0.75 to 1.25 in 2 km grid for the sensitivity analysis (SA), but the results were not analysed spatially. Thus no spatial pattern of sensitivity, showing which zones of the model are more vulnerable to uncertainty, was

HESSD
11, 11987–12025, 2014

obtained. Another spatial approach for SA was presented by Hostache et al. (2010). In their work a local, gradient method was applied to conduct a SA of the Manning coefficient in each mesh of a hydrodynamic model. The results shown completely different sensitivity zonation than in the predefined land-use based Manning coefficient classes.

While most of the research focusses on the rainfall fields, other spatial input data are also interesting, especially since remote sensing data is becoming more and more available. An important spatial parameter for hydrological modelling is imperviousness. The detailed remotely sensed distribution of impervious surfaces was tested against a standard, non-distributed, approach in the WetSpa model (De Smedt et al., 2000; Liu and De Smedt, 2004). Remote sensing based estimation of impervious surfaces showed to have a high sensitivity with respect to runoff prediction (Chormański et al., 2008; Verbeiren et al., 2013) and to give a considerably higher Nash–Sutcliffe efficiencies for discharge simulation as compared to the standard approach (Berezowski et al., 2012). Hence, the WetSpa model showed to be an interesting framework for analysis of spatially distributed phenomena.

Another spatial data set, frequently tested and easier to obtain than rainfall fields, is snow cover. Snow cover fraction (SCF [–]) or snow water equivalent remote sensing products are widely available from a number of sensors. The different available products vary widely in spatial resolution (500 m to 25 km), temporal resolution (sub-daily to monthly) and temporal coverage (the oldest time series starts in 1966, while new products are regularly announced). One of the most frequently used remote sensing snow products comes from the MODIS instrument (Hall et al., 2006). Several studies show different strategies in respect to how hydrological models can benefit from snow cover data. A popular approach is to derive snow depletion curves from MODIS SCF and use them in the Snowmelt Runoff Model – SRM (Martinec, 1975). This approach is still popular and used in recent studies (Lee et al., 2005; Tekeli et al., 2005; Li and Williams, 2008; Butt and Bilal, 2011; Tahir et al., 2011; Bavera et al., 2012). However, the SRM studies are focused mostly on the winter half-year and are limited to study sites where snowmelt processes are dominant. Another popular model which benefit

HESSD
11, 11987–12025, 2014

from satellite derived SCF is HBV (Sælthun, 1996); studies showing use of MODIS snow products are presented by Udnaes et al. (2007) and Şorman et al. (2009). Possibility of using MODIS SCF in the WetSpa model was positively evaluated in Berezowski and Chormański (2011), while MODIS snow products were used to evaluate spatial distribution of predicted snow cover in the WetSpa model (Zeinivand and De Smedt, 2010). The sensitivity of model output to snow cover, despite its popularity as input data in distributed hydrological models, has not yet been evaluated.

The aim of this paper is to provide and test a methodology for a global spatial SA of SCF in a distributed rainfall–runoff model. Purpose of this analysis is to show if the WetSpa model is spatially sensitive to SCF, i.e.: is the uncertainty in different zones of the model dependent on the spatial patterns in the SCF? An important point of the analysis is to explain the existing patterns of spatial sensitivity in function of physical, spatial parameters used and hydrological processes in the study area. For the remainder of the paper, Sect. 2 presents the spatially distributed rainfall–runoff model WetSpa, the study area, data and spatial SA. In Sect. 3 the output of the spatial SA of SCF for Biebrza River catchment is presented and described; the further applicability of the spatial SA method is also discussed in this section. The Sect. 4 presents the main findings of the study.

2 Methods

2.1 Hydrological model

Hydrological simulations were conducted using the WetSpa model (Water and Energy Transfer between Soil, Plants and Atmosphere; De Smedt et al., 2000; Liu et al., 2003). The model divides a catchment into a regular grid with a specified dimension. In each grid cell, the water balance is simulated and the surface, interflow and groundwater discharge components are routed to the catchment outlet (Wang et al., 1996). Spatial parameters used to calculate the hydrological processes are obtained from land-use,

HESSD
11, 11987–12025, 2014

soil and elevation input maps. Attribute tables based on literature data are linked to the maps and transformed to distributed physical values via a GIS preprocessing step (Chormański and Michałowski, 2011). Several studies have demonstrated that WetSpa and its steady state version WetSpass (Batelaan and De Smedt, 2007) are suited to integrate distributed remote sensing input data in the simulation of the hydrological processes (Poelmans et al., 2010; Dujardin et al., 2011; Ampe et al., 2012; Chormański, 2012; Demarchi et al., 2012; Dams et al., 2013).

The model consist of the following storages: interception, depression, root zone, interflow and groundwater. Water transport between the storages is based on physical and empirical equations. Rainfall, temperature and potential evapotranspiration based on data from meteorological stations are made spatially explicit by use of Thiessen polygons, but also a spatially distributed input form is possible.

In the standard WetSpa version, snow accumulation is calculated based on precipitation and a threshold temperature t_0 [°C]. If the temperature in a grid cell is t [°C] and falls below t_0, precipitation is assumed to be snow. Snow melt is calculated based on t_0, a degree-day coefficient k_{snow} [mm °C^{-1}] and coefficient k_{rain} [mm (mm °C)$^{-1}$] reflecting the amount of snowmelt caused by rainfall v_{rain} [mm]. In this study SCF was obtained from MODIS snow products and used as input data. Thus, snow accumulation was not calculated, but replaced with the input SCF, while the snowmelt amount (v_{sm}) [mm day^{-1}] is calculated as:

$$v_{\text{sm}} = \text{SCF}(k_{\text{snow}}(t - t_0) + k_{\text{rain}} v_{\text{rain}}(t - t_0)). \quad (1)$$

This approach of calculating snowmelt based on SCF and snowmelt rate was proposed by Liston (1999). It allows to obtain a distributed v_{sm} values weighted by SCF from grid cells where SCF > 0. WetSpa is also capable to use an energy balance model for snowmelt calculation (Zeinivand and De Smedt, 2010), however, because of the higher demand on input data, this approach was not used.

Surface water routing is based on a geomorphological instantaneous unit hydrograph (IUH) (Liu et al., 2003). The IUH is calculated for a flow path starting in a grid cell

HESSD
11, 11987–12025, 2014

and ending at the catchment outlet, i.e. each grid cell has its own IUH. Groundwater flow and interflow are calculated on a sub-catchment level based on a linear reservoir method and routed to the catchment outlet with the IUH. Comparison of the WetSpa performance with other distributed hydrological models can be found in the results of the DMIP2 project (Safari et al., 2012).

The model was setup with a daily time step and 250 by 250 m grid cells. The calibration period was 1 September 2008 till 31 August 2009, while validation was from 1 September 2007 till 31 August 2008. The length of the calibration and validation was selected to optimize the model for snow conditions occurring in the period selected for SA (Sect. 2.4.3). The global WetSpa parameters were calibrated using the Shuffled Complex Evolution algorithm (Duan et al., 1993). The calibration was conducted with the R software (R Development Core Team, 2013) and package "hydromad". The model was optimized to maximize the Nash and Sutcliffe (1970) efficiency (NS):

$$\mathrm{NS} = 1 - \frac{\sum_{x=1}^{\tau} \left(Q_x - \hat{Q}_x\right)^2}{\sum_{x=1}^{\tau} \left(Q_x - \overline{Q}\right)^2} \quad (2)$$

where: Q_x and $\hat{Q}_x$ are observed and simulated discharges at time x, $\overline{Q}$ is the mean observed discharge, τ is the total number of time steps. Sensitivity of the WetSpa model to the global parameters is presented in Yang et al. (2012).

2.2 Study area

The study area is the Biebrza River catchment upstream from the discharge station at Burzyn. The total catchment area comprises 6845 km^2 (Fig. 1). Biebrza is a lowland catchment consisting of moraine plateaus and post-glacial valleys with low slopes (average 1.03 %, Fig. 2) and an elevation ranging from 102 m a.s.l. at the catchment outlet to 298 m a.s.l. at the northern water divide. Land-use is composed of agriculture

HESSD
11, 11987–12025, 2014

(54 %), forests (26 %), wetlands and grasslands (17 %), water (2 %) and urban (1 %) (Fig. 3). The area is considered as semi-natural, especially because of its large area of well preserved wetlands and forests and is therefore used as a reference area in wetlands research (Wassen et al., 2006). Dominant soil textures in the study area are sand (34 %), loamy sand (26 %) and sandy loam (18 %), whereas minor parts are covered by sandy clay (4 %) and silt (2 %), other soils cover less than 1 % of the area. In the river valley, organic soils are frequent and cover in total 16 % of the study area (Fig. 4).

The Biebrza River is characterized by a spring flood regime, the discharge of the spring flood is mostly related to the volume of snowmelt in the catchment (Stachý, 1987; Mioduszewski et al., 2004; Chormański and Batelaan, 2011). Based on the meteorological record from 25 stations and the flow record at the Burzyn profile (Fig. 1) managed by Polish Institute of Meteorology and Water Management – National Research Institute (IMGW) the study area can be characterized by the following figures. Mean yearly discharge (1951–2012) at Burzyn is 34.9 $m^3 s^{-1}$, while summer and winter average are respectively 26.0 and 43.9 $m^3 s^{-1}$. Recorded extreme low and high discharges (1951–2012) are 4.33 and 517 $m^3 s^{-1}$, respectively. The climate in this area is transitional between continental and Atlantic, with relatively cold winters and warm summers, effectively making this area the coldest region in Poland. The mean air temperature (1979–2009) is 7.0 °C, in the winter half-year 0.3 °C and in the summer half-year 13.7 °C. The mean monthly temperature (1979–2009) has a maximum in July (17.6 °C) and minimum in January (−3.3 °C). The yearly precipitation (1979–2009) is 587 mm (375 mm in the summer half-year, 212 mm in the winter half-year). The yearly average number of days with temperature below 0 °C (1979–2009) is 79 and with snow cover (1975–2012) is 93 (average snow depth is 12 cm). Based on the meteorological maps (Stachý, 1987; Rojek, 2000), the mean yearly evaporation from free water surface (1951–2000) is 550, 465 mm in summer and 85 mm in winter (1951–1970).

HESSD
11, 11987–12025, 2014

2.3 Data

Hydrometeorological data (precipitation, air temperature and discharge) was obtained from IMGW. Daily precipitation was obtained for 25 rain gauge stations, whereas air temperature was available for 5 stations (Fig. 1). Temperature was recorded as minimal and maximal daily temperature, an average from these values was calculated to obtain the mean daily temperature for each station. Daily discharge was obtained for Burzyn. Potential evapotranspiration was estimated based on mean monthly evaporation from free water surface (Stachý, 1987) and uniformly disaggregated into daily values.

Daily SCF was obtained from MODIS/TERRA snow product MOD10A1 (Hall et al., 2006, datasets used: IX 2007 to X 2009) with a 500 m resolution. The SCF values in MOD10A1 are calculated based on the Normalized Difference Snow Index (NDSI):

$$\mathrm{NDSI} = \frac{r_{\mathrm{vis}} - r_{\mathrm{ir}}}{r_{\mathrm{vis}} + r_{\mathrm{ir}}} \tag{3}$$

with r_{vis} and r_{ir} the reflectance in visible and in near-infrared bands, which for the MODIS sensor is respectively band 4 (545–565 nm) and band 6 (1628–1652 nm). In general, NDSI gives higher values if a larger part of a pixel is covered by snow. However, it may be affected by noise from many sources and has to be corrected for bias in forest areas (Klein et al., 1998). The MOD10A1 SCF input data was aggregated into 524 4 by 4 km snow zones, while zones close to the catchment boundary are fractions of a 4 km square. Purpose of the aggregation was to decrease computation time of the SA and to reduce noise in the MOD10A1 data while keeping enough variability to obtain meaningful spatial results. In order to remove missing data related to cloud cover occurrence the SCF in snow zones was linearly interpolated in time. Finally, SCF was set to 0 in months when there was no snow record in lowland Poland, i.e. from May to September.

Spatial data (elevation, land-use and soil) used to calculate distributed model parameters were obtained from variable GIS sources. The elevation map (Fig. 1) was compiled from three sources: Digital Elevation Model of Poland in scale 1 : 26 000,

HESSD
11, 11987–12025, 2014

digitized contours from the Topographical Map of Poland in scale 1 : 25 000 and from filed surveys in the Biebrza valley. The land-use map (Fig. 3) was obtained from the Corine Land Cover 2006 project (Commission of the European Communities, 2013). In the catchment area outside the Polish border (56 km^2), agricultural land-use was assigned. The soil map (Fig. 4) was obtained from the Soil Map of Poland in scale 1 : 50 000 for agricultural areas and 1 : 500 000 in forests and cities. Outside the Polish border the most frequent in the neighbourhood, sandy soil, was assigned. All the spatial data were interpolated to 250 m grid cells using the nearest-neighbourhood (soil, land-use) and the bilinear (elevation) algorithms.

2.4 Sensitivity analysis

2.4.1 Latin-Hypercube One-factor-At-a-Time

Latin-Hypercube One-factor-At-a-Time (LH-OAT) (van Griensven et al., 2006) is an effective global sensitivity analysis method, similar to the Morris screening (Morris, 1991). The LH-OAT method is frequently used by SWAT users for ranking the the parameters according to their influence on the model output (Nossent and Bauwens, 2012). LH-OAT combines two different techniques. First, it selects n latin-hypercube (McKay et al., 1979) samples. Next, the LH points are used as starting points of p one-factor-at-a-time perturbations, where p is equal to the number of model parameters. A higher number of LH samples (n) will lead to a better convergence; a value of at least $n = 100$ is necessary to achieve convergence (Nossent, 2012; Nossent et al., 2013). The method requires in total $p(n+1)$ model evaluations to calculate the SA results. The sensitivity measure (final effect) for each ith parameter is calculated by averaging partial effects for this parameter ($s_{i,j}$) from all LH samples (van Griensven et al., 2006):

$$s_{i,j} = \left| \frac{100\left(\frac{F(e_1,\ldots,e_i(1+f_i),\ldots,e_P)-F(e_1,\ldots,e_i,\ldots,e_P)}{[F(e_1,\ldots,e_i(1+f_i),\ldots,e_P)+F(e_1,\ldots,e_i,\ldots,e_P)]/2}\right)}{f_i} \right| \quad (4)$$

HESSD
11, 11987–12025, 2014

$$s_i = \frac{\sum_{j=1}^{n} s_{ij}}{n} \quad (5)$$

where $F(\cdot)$ is a response or objective function of a model run with a set of e_1 to e_P parameters, e_i is the current parameter, j is the current LH sample; f_i is the fraction by which e_i was changed during the OAT perturbation. s_i should be interpreted as a response measure of the changes in SCF in the snow zones to the value of $F(\cdot)$, a higher sensitivity stands for a stronger response and means that a snow zone is more vulnerable to uncertainty.

2.4.2 Response functions

In order to investigate the relationship between parameters and different model processes, the SA was performed for a set of response functions (RF) $F(\cdot)$. A RF quantifies a model behaviour, but unlike an objective function a RF does not use observation (e.g. observed discharge). Table 1 lists the 15 RF's which were used in the SA. This selection of RF's allows to interpret the results in view of different components of the discharge as simulated by a number of model processes related to them. Moreover, the division into winter and summer half-years gives more insight into seasonal variability of the simulated results. The winter half-year response functions reflect processes occurring during snow accumulation and spring snowmelt, when the highest flows occur. On the other hand, the summer half-year response functions reflect processes occurring during the summer low flow period. Winter half-year RF were calculated for November until April, summer half-year RF for May until October. The $\overline{q}_{\text{high}}$ and $\overline{q}_{\text{low}}$ reflect processes related to the highest and lowest flows. The $\overline{v}_{\text{sm}}$ is calculated as the mean daily value of snowmelt [mm] and reflects processes related to snowmelt generation without routing.

HESSD
11, 11987–12025, 2014

2.4.3 Spatial approach

Usually a SA is performed for global parameters of a model (i.e. a set of parameters valid for the whole model area). The SA presented in this paper however follows a spatial approach, i.e. parameters are evaluated in different zones of the model area, as the parameter e_i represent a fraction of the mean daily MOD10A1 SCF in the model catchment. Each e_i is assigned to one of the 524 snow zones. The resulting spatial distribution is random, but the dynamics of snowmelt and accumulation in time are preserved as in the observed MOD10A1 data. The example of LH-OAT loops for spatial SA is presented in Fig. 5. This study design allows to obtain SCF sensitivity in each snow zone of the model. The set of RF (Table 1) gives further insights into model sensitivity while simulating different processes.

Since the small snow zones at the catchment border would give relatively smaller sensitivity than similarly parametrized zones of bigger area, the s_i measure has to be normalized for non equal area (a_i) of snow zones:

$$\overset{\star}{s}_i = \frac{s_i}{a_i} \tag{6}$$

with $\overset{\star}{s}_i$ the normalised sensitivity. The experimental set-up for the spatial sensitivity was as follows. The values of the global parameters of the WetSpa model where the same as obtained from the model calibration. To be able to achieve convergence, a relatively large number of LH samples was selected (n = 100). Together with the parameters representing the snow zones, p = 524, this results in a total number of model evaluations of 52 500. The LH samples are taken from a uniform distribution ranging from 0 to 1.14, resulting in a range of 0 to 1 for the SCF in a snow zone (maximum mean SCF in the catchment was 88 %, thus $\frac{1}{0.88}$ = 1.14). The perturbation f_i was set to 1 %, in order to avoid that the OAT samples exceed the average distance between the LH samples. The SA was run for two full hydrological years from 1 November 2007 till 31 October 2009, preceded by a warm-up period of 2 months.

HESSD
11, 11987–12025, 2014

2.4.4 Output data analysis

The spatial approach followed in this study gives a large output data set i.e. sensitivity maps based on different RF. Each sensitivity map was analysed in view of 15 WetSpa parameter maps presented in Table 2. The Thiessen polygons for potential evapotranspiration were omitted, as there was only one polygon for the whole catchment.

In order to prepare the dataset for statistical analysis, each of the 15 parameter maps was spatially aggregated to fit the spatial extent of the SA results ($\overset{\star}{s}_i$) – the snow zones by calculating the mean (for continuous data) or the majority (for discrete data) of a parameter value in a snow zone. Based on this data set the coefficient of determination (ρ^2) was calculated for each pair of $\overset{\star}{s}_i$ and the aggregated parameter values. The ρ^2 describes the strength of the linear association between the variables by indicating the fraction of one variable's variance explained by the second variable. Since in literature the thresholds of ρ^2 for quantifying the strength of the linear association are vague, in this paper a $\rho^2 \geq 0.40$ is used as representing a moderate association. The selected threshold is justified by the fact that the $\rho^2 = 0.40$ is equivalent to the Pearson's correlation coefficient of 0.63, which is generally considered as representing a strong relationship between variables.

3 Results and discussion

3.1 Model calibration and performance

The calibrated model shows a good performance with NS = 0.86 for the calibration period, NS = 0.73 for the validation period and NS = 0.79 for the whole period. The comparison of observed and simulated discharge is presented in Fig. 6. 90 % of the simulated discharge at the catchment outlet has a groundwater origin, while surface runoff (5.3 %) and interflow (4.7 %) contribute mostly to the highest peaks (Fig. 6), which is in qualitative agreement with Pajnowska et al. (1984). The model performed

HESSD
11, 11987–12025, 2014

very well during snowmelt-supplied spring floods. The peaks were underestimated by 8 % of the observed value on average, but the shape of the events resembled very well the observed values, which can be an advantage of using observed SCF data instead of predicting snow cover in the model. This is supported by the comparison of the hydrograph (upper part of Fig. 6) with the timing of snowmelt and temperature rise above 0 °C (lower part of Fig. 6), which shows a rapid discharge rise at the beginning of spring floods. Good results of using MODIS snow products in other hydrological models have also been shown by Lee et al. (2005), Udnaes et al. (2007), Şorman et al. (2009) and Tahir et al. (2011). The model performed worse during periods of intensive summer storms. For these storms, a rapid discharge rise was simulated, which was not observed in reality. A possible reason for this low performance is the positively biased soil moisture prediction of the model during these periods.

3.2 Spatial sensitivity analysis

The maps presenting model output sensitivity $\overset{\star}{s}$ (with different RF) to variations of SCF are presented in Fig. 7. The use of different RF results in different patterns of spatial sensitivity, although some similarities can be distinguished. The minimum, maximum and mean values are indicated on each map (Fig. 7). These values are however obtained for different RF and can therefore not be compared with each other. Nevertheless, if the minimum is equal to 0, the model is completely insensitive in at least one snow zone for this RF. The analysis of ρ^2 values (Table 3) explains the spatial relations between SCF sensitivity with different RF and the spatial parameters. Most of the pairs in Table 3 have low ρ^2 indicating that a parameter was not relevant for sensitivity with this RF. However, for most of the RF at least one $\rho^2 \geq 0.40$ was found, indicating that the SCF sensitivity with these RFs can be partially explained by the values of the parameter maps. The values of ρ^2 show influential and unimportant spatial parameters for the SCF sensitivity i.e. for the snow related processes. Another aspect of the results, when looking at the spatial sensitivity patterns, is that higher sensitivity areas are

HESSD
11, 11987–12025, 2014

more vulnerable to uncertainty in the input data. This feature can be used to highlight the areas which require more attention during the parametrization.

3.2.1 General relations of the spatial SA results with parameters maps

Table 3 shows the frequency of the parameters with moderately strong coefficient of determination under different RFs. The most frequent occurring parameter with a coefficient of determination above the threshold (0.40) is slope (slp). slp is very important for calculating hydraulic parameters (e.g. Manning coefficient), but also tunes values of depression storage and potential runoff coefficient. The scatter plots of slp against different RFs (Fig. 8) shows that this parameter explains nearly linear spatial sensitivity quantified with $\overline{q}$, $\overline{qi}$ and $\overline{qg}$ and their winter/summer half-years equivalents. However, when looking closer at the plots for these RFs the lower values of slp (0.0–0.5 %) give steeper relation with less scatter than higher slp values. This means that even when ρ^2 values are high (Table 3), the spatial sensitivity can be explained by a given parameter only in a certain range of its values, while for the remaining values the correlation is not that strong.

The second most frequent is the group of soil texture related parameters: wilting point (w_p), hydraulic conductivity (h_con), porosity (por), residual soil moisture (res) and field capacity (f_c). These parameters have an influence on directing water that is stored as soil moisture, thus have general impact on groundwater, interflow and infiltrability. The soil texture related parameters have higher frequencies than the land-use related parameters (cf. Tables 2 and 3). This means that soil texture is a clearly more important WetSpa input than land-use with regard to the SCF sensitivity. The reason may be that the groundwater discharge accounts for 90 % of the total simulated discharge and the parametrization of the groundwater processes is strongly dependent on soil properties.

The lowest frequency is observed for maximal and minimal interception (i_max and i_min), initial soil moisture (i_sm) and root depth (r_d). For the i_max and i_min the explanation is that the interception capacity is important in the summer half-year, when

HESSD
11, 11987–12025, 2014

no SCF is present. A similar explanation holds for the r_d evapotranspiration parameter, which has a relatively negligible importance in the winter half-year. In case of i_sm, the low frequency may be related to the fact that initial soil moisture content affect mostly the beginning of the simulation, i.e. the warm-up period.

Low frequency is also observed for runoff coefficient (r_c) and depression storage (dep), which are, among others, the most important parameters responsible for generating surface runoff. The low frequencies of these parameters is explained by the fact that the catchment is not urbanized and areas of high r_c and low dep are not frequent in this area. This situation is expected to be different for urbanized catchments, where the surface runoff would participate more in the total discharge than in this study area (Berezowski et al., 2012).

The frequency analysed in this subsection is obviously dependent on the value of the ρ^2 threshold (in this case 0.40). The threshold is subjective, however, discriminates well between the high and low ρ^2. Nevertheless, the results should be viewed also in scope of the ρ^2 values themselves.

3.2.2 Discharge source response functions

All the sensitivity maps calculated for the winter half-year RF resemble the full year RF, both in the ρ^2 (Table 3) and in the spatial pattern (Fig. 7). This means that when looking at SCF sensitivity, the winter processes dominate the whole year. The reason for this lies in the fact that snowmelt water is routed mostly in winter and spring, while in summer water routing is only affected by remaining snowmelt water in soil moisture and groundwater reservoirs.

Using $\overline{q}$ and $\overline{q}_w$ as RF resulted in a clear pattern differentiating the upland from the valley (cf. Figs. 7 and 9), showing that SCF zones occurring in the flat, organic-soil dominated valley is much less sensitive than in the mineral upland. High sensitivity is obtained in snow zones with steeper slopes (cf. Figs. 7 and 2), what is confirmed by high ρ^2 with slp (Table 3). Several WetSpa parameters (mostly soil texture dependent dep, w_p, f_cap, por, res) have high ρ^2 with these RFs (Table 3), which identifies

HESSD
11, 11987–12025, 2014

a strong link between SCF sensitivity and general model behaviour. Moreover, this confirms the suitability of WetSpa for the selected study area and processes occurring within it. The parameters with lowest ρ^2 were: i_max, i_min and r_d, which are responsible for processes in summer half-year.

Some differences between $\overline{q}$ and $\overline{q}_s$ are visible when analysing the relationship strength (Table 3). The SCF sensitivity for $\overline{q}_s$ has stronger relationship with parameters important for groundwater processes, like: por, res, f_cap and pore size distribution index (p_ind). Thus, the SCF appears to influence summer half-year discharges more by groundwater than by surface runoff.

When comparing $\overline{q}$, $\overline{q}_w$ and $\overline{q}_s$ with $\overline{qg}$, $\overline{qg}_w$ and $\overline{qg}_s$ with respect to spatial patterns (Fig. 7) and ρ^2 (Table 3), the figures are very similar. Obviously, the group of parameters responsible for groundwater processes (por, res, f_cap and p_ind) have higher ρ^2 with the groundwater RF's $\overline{qg}$ and $\overline{qg}_w$ than with $\overline{q}$ and $\overline{q}_w$. It is clear that the groundwater discharge dominates the total discharge in the model of Biebrza River catchment when looking at the similar results for the total discharge and groundwater discharge RF. This result is also confirmed in functioning of the Biebrza River catchment as described in literature (Pajnowska et al., 1984; Batelaan and Kuntohadi, 2002; Wassen et al., 2006; Chormański et al., 2011a).

The SCF sensitivity for $\overline{qs}$ and $\overline{qs}_w$ differentiates the river valley and the north-western upland catchment from the south-eastern upland (cf. Figs. 7 and 9). This sensitivity pattern may be related to the soil properties. As presented in Fig. 4, the SE upland is dominated by loamy sand (h_con = 1.7×10^{-5} m s^{-1}), while much lower hydraulic conductivities are observed in the river valley (dominated by organic soils h_con = 5.6×10^{-6} m s^{-1}) and the NW upland (big share of sandy loam h_con = 6.9×10^{-6} m s^{-1}). The soil-sensitivity pattern is confirmed by the high ρ^2 with h_con and weak, but noticeable ρ^2 with r_c. The infiltration ability and surface water routing, plays an important role in explaining the SCF sensitivity for surface runoff. The maps of SCF sensitivity for $\overline{qs}$ and $\overline{qs}_w$ are the only one that show clearly a relatively higher sensitivity in the river valley than in most of the upland. This may be related to the

HESSD
11, 11987–12025, 2014

fact that snowmelt in the Biebrza River valley is a considerable water source to spring floods and is transported as surface runoff (Chormański et al., 2011b).

The SCF sensitivity for $\overline{qs}_s$ shows a similar pattern as for $\overline{qs}$, but faded (Fig. 7). As mentioned before, summer runoff is only influenced by SCF through antecedent soil moisture conditions, which in case of $\overline{qs}_s$ may be linked to the strong relationship with p_ind.

The SCF sensitivity for the interflow RF differs from the groundwater and surface water RF results. The spatial pattern of SCF sensitivity for $\overline{qi}$ and $\overline{qi}_w$ seems opposite to the pattern of $\overline{qs}$ and $\overline{qs}_w$. In the WetSpa model the interflow depends not only on h_con (the key parameter for explaining sensitivity for $\overline{qs}_w$), but also on slp, which is important for routing water in the subsoil and, thus shows high ρ^2 with SCF sensitivity for $\overline{qi}$ and $\overline{qi}_w$.

No $\rho^2 \geq 0.40$ are found for the SCF sensitivity for $\overline{qi}_s$ (Table 3). In this case, the role of the parameters is limited. This is probably because most of the interflow water that could be related to SCF produced discharge during winter half-year. The highest ρ^2, similarly like for $\overline{qi}$ and $\overline{qi}_w$, is found with slp, which can also be easily linked by similarity of spatial patterns with the SCF sensitivity map (cf. Figs. 2 and 7).

3.2.3 Extreme discharges response functions

The SCF sensitivity for $\overline{q}_{high}$ presents a spatial pattern that can not be visually related to land-use, soil, or slope maps (Fig. 7). The spatial pattern shows high values both in the upland and in the valley, however it has also some zones of low sensitivity in the central part of valley. Low but noticeable ρ^2 is found with slp indicating a link with runoff generation in WetSpa. Thus slp may directly influence the 10 % highest discharges and the SCF sensitivity. Nevertheless there are other sources of variance in the SCF sensitivity for $\overline{q}_{high}$, which do not have an origin in the parameter maps. Detailed precipitation conditions and timing is e.g. not fully reflected by the aggregated precipitation P.

HESSD
11, 11987–12025, 2014

The spatial pattern of SCF sensitivity for $\overline{q}_{low}$ is quite uniform, with some higher values in the western uplands, lower values in the central part of the valley and in flat regions in the northern upland (cf. Figs. 9 and 7). The pattern of $\overline{q}_{low}$ may also be related to extreme groundwater deficits to which mineral soils in the uplands have a higher contribution than organic saturated soils in the valley (por has low, but noticeable ρ^2). The spatial pattern of soil moisture in the Biebrza River valley presented by Dabrowska-Zielińska et al. (2009) partially confirms the spatial SA results presented in this paper.

3.2.4 Mean snowmelt response function

A completely different pattern than for the other RF is presented by SCF sensitivity for $\overline{v}_{sm}$ (Fig. 7). According to the Eq. (1), v_{sm} in a model grid cell (and thus $\overline{v}_{sm}$ in the entire catchment) is calculated based on temperature and precipitation, and then adjusted by SCF. Hence, the sensitivity for $\overline{v}_{sm}$ corresponds with the spatial pattern of the mean yearly temperature averaged in the Thiessen polygons (T), while yearly sum of precipitation in the Thiessen polygons (P) is less influential. The pattern of SCF is not visible, because in this analysis the SCF values in Eq. (1) come from the random LH-OAT sampling. The reason that ρ^2 between v_{sm} and T and P is lower than 1.00 is because the values are aggregated in time and space and lose some of the variance important for the relation.

3.3 Applicability of the spatial SA

The analyses conducted in this case study are both a validation and an example application of spatial SA method. The further potential use of this method could be twofold: for generic sensitivity analysis and for a catchment change scenario analysis.

The generic sensitivity analysis would be similar to the presented approach in this paper. The sensitivity maps (e.g. Fig. 7) would show zones of the catchment with high sensitivity. The correlation analysis as in Table 3 would show the parameters explaining

HESSD
11, 11987–12025, 2014

the sensitivity pattern which thus require more attention during the parametrization. This would require possibly denser field sampling of the correlated parameters, or obtaining the parameters form a source with less uncertainty; as a result the prediction uncertainty would be decreased. Additionally, the detailed scatter plots of parameters against RFs (e.g. Fig. 8) would show which data ranges of the parameters are the most responsible for the spatial sensitivity pattern. In contrast the "standard" SA is performed for global parameters which usually are not spatially distributed, or are semi-distributed (i.e. grouped to few categories with the same values; e.g. Ayvaz, 2013).

The catchment change scenario analysis was not investigated in this paper but is a possible application of the presented spatial SA algorithm. In such an analysis instead for SCF input time series the LH-OAT sampling would be done for e.g. different land covers proportions in the catchment zones. The output of such an analysis would be sensitivity of the zones to changes in land cover and could be used as e.g. a stochastic decision support for urban development.

4 Conclusions

With increasing spatial data availability for distributed hydrological modelling a need appears for a methodology for sensitivity analysis of the spatial data. Such a methodology should point to zones of the study area where the sensitivity of a model spatial input to output is higher or lower and should relate these patterns to the processes simulated by the model. In order to answer these needs this paper presents an application of the LH-OAT sensitivity analysis to the WetSpa model of the Biebrza River catchment. Unlike a standard SA of global model parameters, a spatial approach is presented in this study. The catchment is divided into regular snow grid cells or zones in which sensitivity of SCF as input data was evaluated. The aim of this study was to present an approach for using SA for spatial input data and to show that the WetSpa model is sensitive to spatial input data. Moreover, it was intended to show that the spatial sensitivity results are related to physical parameters used in the model.

HESSD
11, 11987–12025, 2014

The spatial approach of the LH-OAT SA results in spatial maps presenting areas of relatively higher and lower sensitivity. In order to extend the analysis, the SA was repeated with different response functions (RF). Most of the SA results were similar for the whole year and winter-half year RF. Moreover, the sensitivity obtained for the mean discharge RF was very similar to the SA for the mean groundwater discharge RF. Hence, the snow-processes related model behaviour is dominated by winter half-year and groundwater processes, which is in agreement with the Biebrza River spring flood regime with a dominant share of groundwater discharge. Another important finding was that SCF sensitivity was high in snow zones in the river valley under the winter half-year surface runoff RF. This is in agreement with the observation that the snowmelt in the river valley is a considerable surface runoff source to spring floods.

In this case study, the spatial patterns of SCF sensitivity could, for most of the RF, easily be interpreted by co-occurrence of different landscape features like upland and river valley. However, for some of the RF a straightforward interpretation was impossible. A successful approach to interpret the patterns was performed by analysing the values of coefficients of determination between the physical model parameters and the SCF sensitivity. The spatial pattern of the sensitivity for different RF, obtained from these results, is related to different spatial parameters and to different physical processes simulated by the model. The parameters which had a strong relationship with the SCF sensitivity for most of the RF were: slope, and the soil related parameters. The potential runoff coefficient and depression storage were important for only a few RF's, because the catchment is not urbanized. The temperature, which directly influences the snowmelt generation in the WetSpa model, shows a strong relationship only with the mean snowmelt RF. It is important to mention that the spatial sensitivity quantified with several RF's was correlated to more than one spatial parameter. This shows the importance of the links between the parameters and which were revealed by this spatially distributed analysis.

In summary, a spatial approach of SA can be performed with the LH-OAT algorithm, as presented in the results of this paper, and the SCF is spatially sensitive in

HESSD
11, 11987–12025, 2014

the WetSpa model. The pattern of spatial sensitivity is related to spatially distributed physical parameters, the results are confirmed by priori scientific understanding of the Biebrza River catchment functioning. The spatial sensitivity maps can by used to highlight areas which require better attention during the parametrization and to show which spatial parameters have influence on the analysed phenomena, in this case the snow related processes.

In future work, other input time series or input parameters should be evaluated in a spatial analysis. It would also be interesting to compare spatial sensitivity of the same input data with other models e.g. TOPMODEL or SWAT. Finally, since spatial SCF is sensitive in WetSpa, other sources of this input data should be tested in the model.

Acknowledgements. First author acknowledge Ignacy Kardel for sharing the DEM and sources for the soil map used in this study. First author also acknowledges the Flemish Government for supporting his research visit to the Vrije Universiteit Brussel. The Hydro-meteorological data was provided by Institute of Meteorology and Water Management – National Research Institute (IMGW).

References

Abbott, M., Bathurst, J., Cunge, J., O'Connell, P., and Rasmussen, J.: An introduction to the European Hydrological System – Systeme Hydrologique Europeen, "SHE", 2: Structure of a physically-based, distributed modelling system, J. Hydrol., 87, 61–77, 1986. 11989

Ampe, E., Vanhamel, I., Salvadore, E., Dams, J., Bashir, I., Demarchi, L., Chan, J., Sahli, H., Canters, F., and Batelaan, O.: Impact of urban land-cover classification on groundwater recharge uncertainty, IEEE J. Sel. Top. Appl., 5, 1859–1867, 2012. 11992

Ayvaz, M. T.: A linked simulation-optimization model for simultaneously estimating the Manning's surface roughness values and their parameter structures in shallow water flows, J. Hydrol., 500, 183–199, 2013. 12006

Batelaan, O. and De Smedt, F.: GIS-based recharge estimation by coupling surface-subsurface water balances, J. Hydrol., 337, 337–355, 2007. 11992

HESSD

11, 11987–12025, 2014

Batelaan, O. and Kuntohadi, T.: Development and application of a groundwater model for the Upper Biebrza River Basin, Annals of Warsaw Agricultural University-SGGW, Land Reclam., 33, 57–69, 2002. 12003

Bavera, D., De Michele, C., Pepe, M., and Rampini, A.: Melted snow volume control in the snowmelt runoff model using a snow water equivalent statistically based model, Hydrol. Process., 26, 3405–3415, 2012. 11990

Berezowski, T. and Chormański, J.: Analysis of use of satellite imagery for extraction of snow cover distribution as a parameter in a rainfall–runoff model, Scient. Rev. – Eng. Environ. Sci., 51, 15–26, 2011. 11991

Berezowski, T., Chormański, J., Batelaan, O., Canters, F., and Van de Voorde, T.: Impact of remotely sensed land-cover proportions on urban runoff prediction, Int. J. Appl. Earth Obs., 16, 54–65, 2012. 11990, 12002

Beven, K. and Freer, J.: A dynamic TOPMODEL, Hydrol. Process., 15, 1993–2011, 2001. 11989

Beven, K., Lamb, R., Quinn, P., Romanowicz, R., Freer, J., and Singh, V.: Topmodel, Computer Models of Watershed Hydrology, Water Resource Publications, Colorado, USA, 627–668, 1995. 11989

Butt, M. J. and Bilal, M.: Application of snowmelt runoff model for water resource management, Hydrol. Process., 25, 3735–3747, 2011. 11990

Chormański, J.: Analysis of urbanization impact on changes in river discharge – a case study of the Biała river catchment, Studia Geotechnica et Mechanica, 34, 19–32, 2012. 11992

Chormański, J. and Batelaan, O.: Application of the WetSpa distributed hydrological model for catchment with significant contribution of organic soil. Upper Biebrza case study, Annals of Warsaw University of Life Sciences-SGGW, Land Reclam., 43, 25–35, 2011. 11994

Chormański, J. and Michałowski, R.: Hydrological catchment model WetSpa-SGGW integrated with a calculation module in ArcGIS environment, Scient. Rev. – Eng. Environ. Sci., 53, 196–206, 2011. 11992

Chormański, J., Van de Voorde, T., De Roeck, T., Batelaan, O., and Canters, F.: Improving distributed runoff prediction in urbanized catchments with remote sensing based estimates of impervious surface cover, Sensors, 8, 910–932, 2008. 11990

Chormański, J., Berezowski, T., Okruszko, T., and Ignar, S.: Hydrography and hydrology of the upper Biebrza basin, in: Contemporary Problems of Management and Environmental

HESSD
11, 11987–12025, 2014

Protection, vol. 7, Issue of Landscape Conservation and Water Management in Rural Areas, Uniwersytet Warminsko Mazurski, Olsztyn, 175–203, 2011a. 12003
Chormański, J., Okruszko, T., Ignar, S., Batelaan, O., Rebel, K., and Wassen, M.: Flood mapping with remote sensing and hydrochemistry: a new method to distinguish the origin of flood water during floods, Ecol. Eng., 37, 1334–1349, 2011b. 12004
Commission of the European Communities: CORINE Land-cover, available at: http://www.eea.europa.eu/publications/COR0-landcover, last access: 1 November 2013. 11996
Dabrowska-Zielińska, K., Gruszczyńska, M., Lewiński, S., Hościło, A., and Bojanowski, J.: Application of remote and in situ information to the management of wetlands in Poland, J. Environ. Manage., 90, 2261–2269, 2009. 12005
Dams, J., Dujardin, J., Reggers, R., Bashir, I., Canters, F., and Batelaan, O.: Mapping impervious surface change from remote sensing for hydrological modeling, J. Hydrol., 485, 84–95, 2013. 11992
Demarchi, L., Canters, F., Chan, J. C.-W., Ampe, E., and Batelaan, O.: Use of land-cover fractions derived from MESMA for urban water balance calculation, in: Geoscience and Remote Sensing Symposium (IGARSS), 2012 IEEE International, IEEE, Munich, Germany, 1594–1597, 2012. 11992
De Smedt, F., Liu, Y. B., and Gebremeskel, S.: Hydrologic modeling on a catchment scale using GIS and remote sensed land use information, in: Risk Analysis II, WTI Press, Southampton, Boston, 295–304, 2000. 11990, 11991
Duan, Q., Gupta, V., and Sorooshian, S.: Shuffled complex evolution approach for effective and efficient global minimization, J. Optimiz. Theor. Appl., 76, 501–521, 1993. 11993
Dujardin, J., Batelaan, O., Canters, F., Boel, S., Anibas, C., and Bronders, J.: Improving surface-subsurface water budgeting using high resolution satellite imagery applied on a brownfield, Sci. Total Environ., 409, 800–809, 2011. 11992
Fu, S., Sonnenborg, T. O., Jensen, K. H., and He, X.: Impact of precipitation spatial resolution on the hydrological response of an integrated distributed water resources model, Vadose Zone J., 10, 25–36, 2011. 11989
Hall, D. K., Riggs, G. A., and Salomonson, V. V.: MODIS/Terra Snow Cover Daily L3 Global 500 m Grid V005, Dataset used 2007–2009, digital media, National Snow and Ice Data Center, Boulder, CO, USA, 2006. 11990, 11995

HESSD
11, 11987–12025, 2014

Hostache, R., Lai, X., Monnier, J., and Puech, C.: Assimilation of spatially distributed water levels into a shallow-water flood model, Part II: Use of a remote sensing image of Mosel River, J. Hydrol., 390, 257–268, 2010. 11990
Klein, A. G., Hall, D. K., and Riggs, G. A.: Improving snow cover mapping in forests through the use of a canopy reflectance model, Hydrol. Process., 12, 1723–1744, 1998. 11995
Lee, S., Klein, A. G., and Over, T. M.: A comparison of MODIS and NOHRSC snow-cover products for simulating streamflow using the snowmelt runoff model, Hydrol. Process., 19, 2951–2972, 2005. 11990, 12000
Li, X. and Williams, M. W.: Snowmelt runoff modelling in an arid mountain watershed, Tarim Basin, China, Hydrol. Process., 22, 3931–3940, 2008. 11990
Liston, G. E.: Interrelationships among snow distribution, snowmelt, and snow cover depletion: implications for atmospheric, hydrologic, and ecologic modeling, J. Appl. Meteorol., 38, 1474–1487, 1999. 11992
Liu, Y. B. and De Smedt, F.: WetSpa Extension, a GIS-based Hydrologic Model for Flood Prediction and Watershed Management, Department of Hydrology and Hydraulic Engineering, Vrije Universiteit, Brussel, 66 pp., 2004. 11990
Liu, Y. B., Gebremeskel, S., De Smedt, F., Hoffmann, L., and Pfister, L.: A diffusive transport approach for flow routing in GIS-based flood modeling, J. Hydrol., 283, 91–106, 2003. 11991, 11992
Martinec, J.: Snowmelt – runoff model for stream flow forecasts, Nord. Hydrol., 6, 145–154, 1975. 11990
McKay, M., Beckman, R., and Conover, W.: Comparison of three methods for selecting values of input variables in the analysis of output from a computer code, Technometrics, 21, 239–245, 1979. 11996
Mioduszewski, W., Querner, E. P., Slesicka, A., and Zdanowicz, A.: Basis of water management in the Valley of Lower Biebrza River, J. Water Land Develop., 8, 49–61, 2004. 11994
Morris, M. D.: Factorial sampling plans for preliminary computational experiments, Technometrics, 33, 161–174, 1991. 11996
Nash, J. and Sutcliffe, J.: River flow forecasting through conceptual models part I: A discussion of principles, J. Hydrol., 10, 282–290, 1970. 11993
Nossent, J.: Sensitivity and uncertainty analysis in view of the parameter estimation of a SWAT model of the river Kleine Nete, Belgium, Ph.D. thesis, Vrije Universiteit, Brussel, 2012. 11996

HESSD
11, 11987–12025, 2014

Nossent, J. and Bauwens, W.: Multi-variable sensitivity and identifiability analysis for a complex environmental model in view of integrated water quantity and water quality modeling, Water Sci. Technol., 65, 539–549, 2012. 11996

Nossent, J., Tolessa Leta, O., and Bauwens, W.: Assessing the convergence of a Morris-like screening method for a complex environmental model, in: 7th International Conference on Sensitivity Analysis of Model Output, Oral presentations Proceedings, Nice, 2013. 11996

Obled, C., Wendling, J., and Beven, K.: The sensitivity of hydrological models to spatial rainfall patterns – an evaluation using observed data, J. Hydrol., 159, 305–333, 1994. 11989

Pajnowska, H., Poźniak, R., and Wiencław, E.: Groundwaters of the Biebrza Valley, Polish Ecol. Stud., 10, 301–311, 1984. 11999, 12003

Poelmans, L., Van Rompaey, A., and Batelaan, O.: Coupling urban expansion models and hydrological models: how important are spatial patterns?, Land Use Policy, 27, 965–975, 2010. 11992

Querner, E.: Description and application of the combined surface and groundwater flow model MOGROW, J. Hydrol., 192, 158–188, 1997. 11989

R Development Core Team: R: a Language and Environment for Statistical Computing, R Foundation for Statistical Computing, Vienna, Austria, 2013. 11993

Rojek, M.: Evaporation from free water surface 1951–2000, Map in scale 1 : 2 500 000, Tech. rep., IMGW, Warsaw, Poland, 2000. 11994

Sælthun, N.: The Nordic HBV Model, Norwegian Water Resources and Energy Administration Publication, Oslo, Norway, 1996. 11991

Safari, A., De Smedt, F., and Moreda, F.: WetSpa model application in the Distributed Model Intercomparison Project (DMIP2), J. Hydrol., 418–419, 78–89, 2012. 11993

Schuurmans, J. M. and Bierkens, M. F. P.: Effect of spatial distribution of daily rainfall on interior catchment response of a distributed hydrological model, Hydrol. Earth Syst. Sci., 11, 677–693, doi:10.5194/hess-11-677-2007, 2007. 11989

Şorman, A. A., Şensoy, A., Tekeli, A. E., Şorman, A. U., and Akyürek, Z.: Modelling and forecasting snowmelt runoff process using the HBV model in the eastern part of Turkey, Hydrol. Process., 23, 1031–1040, 2009. 11991, 12000

Stachý, J.: Hydrological Atlas of Poland, vol. 1, Wydawnictwo Geologiczne, Warsaw, Poland, 1987. 11994, 11995

HESSD
11, 11987–12025, 2014

Stisen, S., McCabe, M. F., Refsgaard, J. C., Lerer, S., and Butts, M. B.: Model parameter analysis using remotely sensed pattern information in a multi-constraint framework, J. Hydrol., 409, 337–349, 2011. 11989

Tahir, A. A., Chevallier, P., Arnaud, Y., Neppel, L., and Ahmad, B.: Modeling snowmelt-runoff under climate scenarios in the Hunza River basin, Karakoram Range, Northern Pakistan, J. Hydrol., 409, 104–117, 2011. 11990, 12000

Tekeli, A. E., Akyürek, Z., Arda Şorman, A., Şensoy, A., and Unal Şorman, A.: Using MODIS snow cover maps in modeling snowmelt runoff process in the eastern part of Turkey, Remote Sens. Environ., 97, 216–230, 2005. 11990

Udnaes, H. C., Alfnes, E., and Andreassen, L. M.: Improving runoff modelling using satellite-derived snow covered area?, Nord. Hydrol., 38, 21–32, 2007. 11991, 12000

van Griensven, A., Meixner, T., Grunwald, S., Bishop, T., Diluzio, M., and Srinivasan, R.: A global sensitivity analysis tool for the parameters of multi-variable catchment models, J. Hydrol., 324, 10–23, 2006. 11996

Verbeiren, B., Van De Voorde, T., Canters, F., Binard, M., Cornet, Y., and Batelaan, O.: Assessing urbanisation effects on rainfall–runoff using a remote sensing supported modelling strategy, Int. J. Appl. Earth Obs., 21, 92–102, 2013. 11990

Wang, Z.-M., Batelaan, O., and Smedt, F. D.: A distributed model for water and energy transfer between soil, plants and atmosphere (WetSpa), Phys. Chem. Earth, 21, 189–193, 1996. 11991

Wassen, M. J., Okruszko, T., Kardel, I., Chormanski, J., Swiatek, D., Mioduszewski, W., Bleuten, W., Querner, E. P., El Kahloun, M., Batelaan, O., and Meire, P.: Eco-hydrological functioning of the Biebrza wetlands: lessons for the conservation and restoration of deteriorated wetlands, Wetlands, 191, 285–310, 2006. 11994, 12003

Yang, J., Liu, Y., Yang, W., and Chen, Y.: Multi-objective sensitivity analysis of a fully distributed hydrologic model WetSpa, Water Resour. Manage., 26, 109–128, 2012. 11993

Younger, P. M., Freer, J. E., and Beven, K. J.: Detecting the effects of spatial variability of rainfall on hydrological modelling within an uncertainty analysis framework, Hydrol. Process., 23, 1988–2003, 2009. 11989

Zeinivand, H. and De Smedt, F.: Prediction of snowmelt floods with a distributed hydrological model using a physical snow mass and energy balance approach, Nat. Hazards, 54, 451–468, 2010. 11991, 11992

HESSD
11, 11987–12025, 2014

Table 1. The descriptions and abbreviations of the 15 RF's which were used in the SA.

Description	RF abbreviation		
	yearly	winter	summer
Mean simulated discharge	$\overline{q}$	$\overline{q}_{\mathrm{w}}$	$\overline{q}_{\mathrm{s}}$
Mean simulated discharge from surface runoff	$\overline{qs}$	$\overline{qs}_{\mathrm{w}}$	$\overline{qs}_{\mathrm{s}}$
Mean simulated discharge from interflow	$\overline{qi}$	$\overline{qi}_{\mathrm{w}}$	$\overline{qi}_{\mathrm{s}}$
Mean simulated discharge from groundwater	$\overline{qg}$	$\overline{qg}_{\mathrm{w}}$	$\overline{qg}_{\mathrm{s}}$
Mean of the highest 10 % simulated discharges	$\overline{q}_{\mathrm{high}}$	–	–
Mean of the lowest 10 % simulated discharges	$\overline{q}_{\mathrm{low}}$	–	–
Mean simulated snowmelt	$\overline{v}_{\mathrm{sm}}$	–	–

HESSD
11, 11987–12025, 2014

Table 2. The WetSpa parameter maps used to analyse the SA results. The generic input maps used to derive the parameters maps are marked with + if used and – if not used.

Parameter	Abbreviation	Generic input map		
		Soil	Land-use	Elevation
Slope	slp	–	–	+
Hydraulic conductivity	h_con	+	–	–
Soil field capacity	f_cap	+	–	–
Maximal interception	i_max	–	+	–
Minimal interception	i_min	–	+	–
Pore size distribution index	p_ind	+	–	–
Soil porosity	por	+	–	–
Residual soil moisture content	res	+	–	–
Root depth	r_d	–	+	–
Wilting point	w_p	+	–	–
Runoff coefficient	r_c	+	+	+
Depression storage	dep	+	+	+
Initial soil moisture content	i_sm	+	–	+
Thiessen polygons for temperature	T		from the stations	
Thiessen polygons for precipitation	P		from the stations	

HESSD
11, 11987–12025, 2014

Table 3. The ρ^2 calculated between the WetSpa distributed parameters (rows) and the SCF sensitivity maps under different RFs (columns). The $\rho^2 \geq 0.40$ are bold; the frequency that this condition is true is summarized (Σ) in the last row and column. Explanation of the RFs and parameters is presented in Tables 1 and 2.

	$\overline{q}$	$\overline{q}_w$	$\overline{q}_s$	$\overline{qs}$	$\overline{qs}_w$	$\overline{qs}_s$	$\overline{qi}$	$\overline{qi}_w$	$\overline{qi}_s$	$\overline{qg}$	$\overline{qg}_w$	$\overline{qg}_s$	$\overline{q}_{high}$	$\overline{q}_{low}$	$\overline{v}_{sm}$	Σ
slp	**0.58**	**0.58**	**0.48**	0.00	0.00	0.02	**0.45**	**0.44**	0.23	**0.56**	**0.56**	**0.45**	0.36	0.12	0.09	8
h_con	0.00	0.00	0.00	**0.40**	**0.40**	0.28	0.16	0.15	0.11	0.00	0.00	0.00	0.01	0.00	0.00	2
f_cap	0.25	0.20	**0.41**	0.15	0.15	0.02	0.24	0.24	0.14	0.27	0.23	**0.40**	0.15	0.18	0.12	2
i_max	0.00	0.01	0.00	0.03	0.03	0.03	0.00	0.00	0.07	0.00	0.00	0.00	0.00	0.00	0.01	0
i_min	0.09	0.07	0.16	0.03	0.03	0.01	0.03	0.04	0.02	0.10	0.08	0.16	0.05	0.02	0.01	0
p_ind	0.09	0.07	0.20	0.21	0.20	**0.42**	0.00	0.00	0.01	0.08	0.06	0.18	0.06	0.18	0.20	1
por	0.25	0.20	**0.44**	0.03	0.04	0.00	0.16	0.16	0.10	0.26	0.22	**0.42**	0.15	0.22	0.17	2
res	0.25	0.20	**0.42**	0.10	0.11	0.01	0.20	0.20	0.12	0.27	0.23	**0.41**	0.15	0.19	0.13	2
r_d	0.00	0.01	0.00	0.12	0.12	0.08	0.00	0.00	0.04	0.00	0.00	0.01	0.00	0.00	0.01	0
w_p	0.25	0.21	**0.42**	0.14	0.14	0.02	0.23	0.23	0.13	0.27	0.23	**0.41**	0.15	0.18	0.12	2
r_c	0.03	0.02	0.11	0.30	0.30	0.12	0.11	0.10	0.04	0.05	0.03	0.12	0.02	0.08	0.06	0
dep	0.26	0.26	0.24	0.11	0.11	0.15	0.05	0.05	0.06	0.24	0.24	0.22	0.14	0.06	0.03	0
i_sm	0.07	0.06	0.10	0.00	0.00	0.00	0.07	0.07	0.00	0.07	0.06	0.10	0.05	0.04	0.00	0
T	0.05	0.05	0.02	0.03	0.03	0.16	0.08	0.09	0.00	0.04	0.05	0.02	0.01	0.00	**0.42**	1
P	0.02	0.03	0.00	0.00	0.00	0.02	0.01	0.01	0.06	0.02	0.03	0.00	0.04	0.08	0.19	0
Σ	1	1	5	1	1	1	1	1	0	1	1	5	0	0	1	

HESSD
11, 11987–12025, 2014

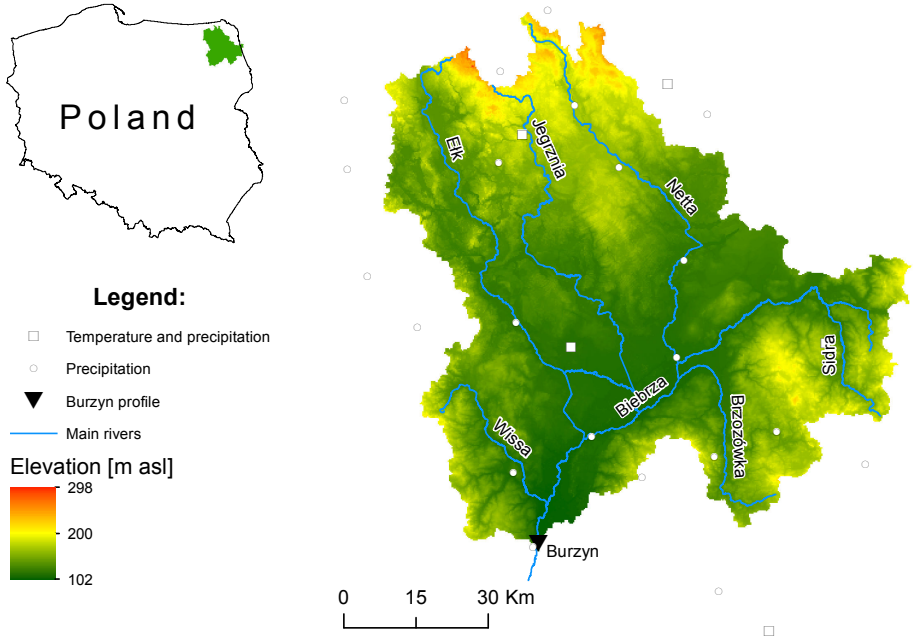

Figure 1. Topography of the study area and location of meteorological stations.

HESSD
11, 11987–12025, 2014

Spatial senitivity analysis of snow cover data

T. Berezowski et al.

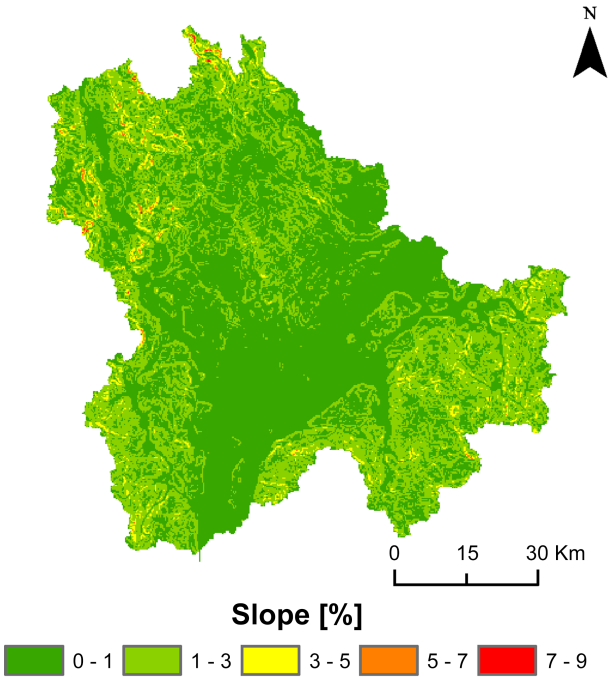

Figure 2. Slope map of the study area.

HESSD
11, 11987–12025, 2014

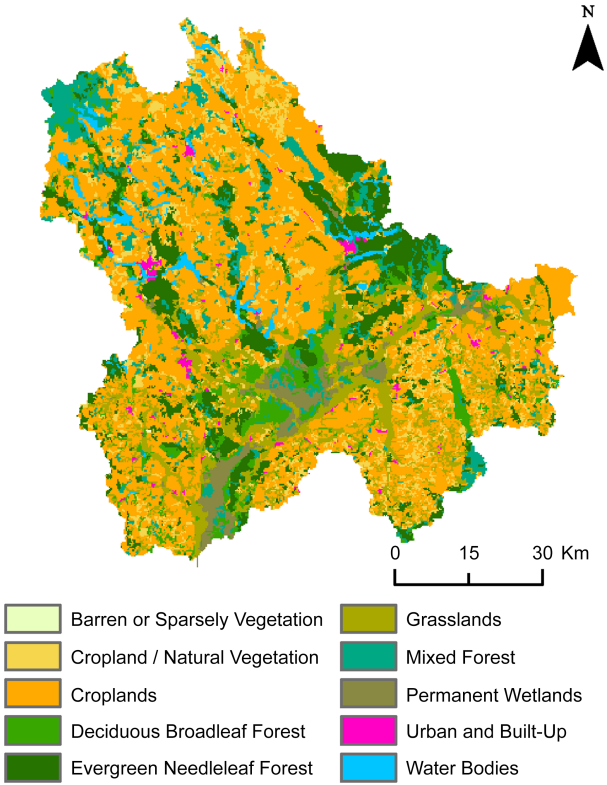

Figure 3. Land-use in the study area. Land-use classes are the same as used in the WetSpa model, defined by International Geosphere-Biosphere Program classification system.

HESSD
11, 11987–12025, 2014

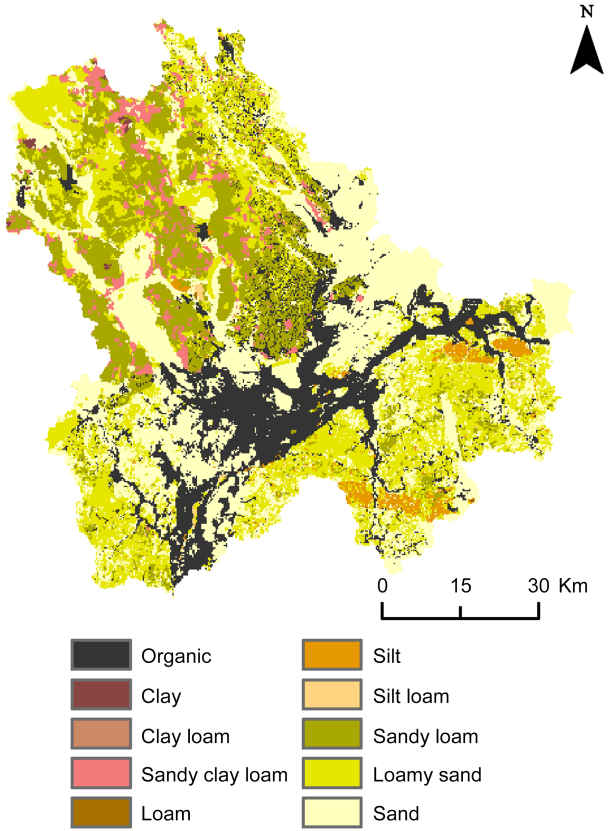

Figure 4. Soil texture map of the study area. Soil textures are the same as used in the WetSpa model, defined by US Department of Agriculture.

HESSD
11, 11987–12025, 2014

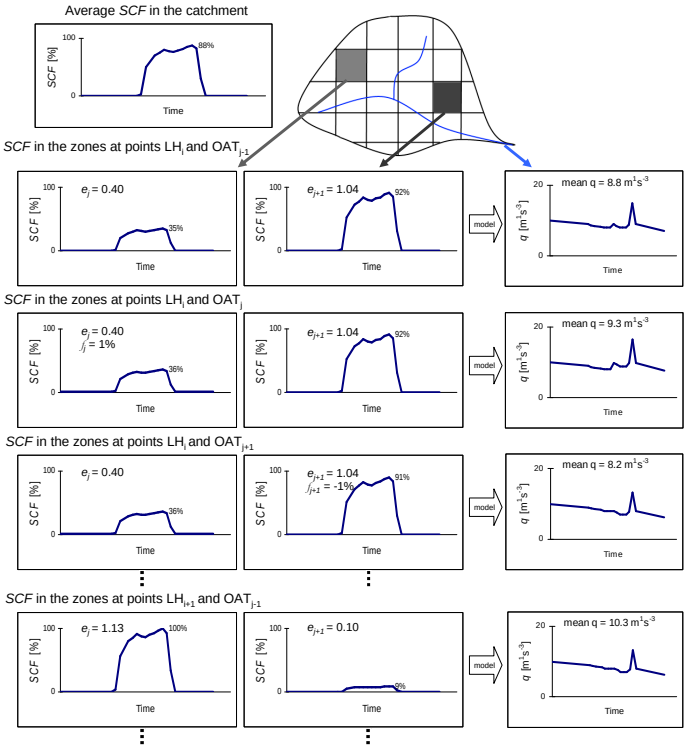

Figure 5. Graph illustrating the spatial LH-OAT SCF sampling for calculating the SA. The top row presents a spatially averaged, observed SCF for an example catchment (left panels) and an example catchment with highlighted snow zones j and $j+1$ (right panels). The next rows presents SCF in the zones j (left column panels) and $j+1$ (central column panels) in the advancing LH-OAT loops starting from the loop $j-1$ and simulated discharge during these loops (right column panels). Symbols are the same as in Eq. (4): e represent a fraction of the SCF, f is the fraction by which e was changed during the OAT perturbation, q is the discharge simulated at the catchment outlet.

HESSD
11, 11987–12025, 2014

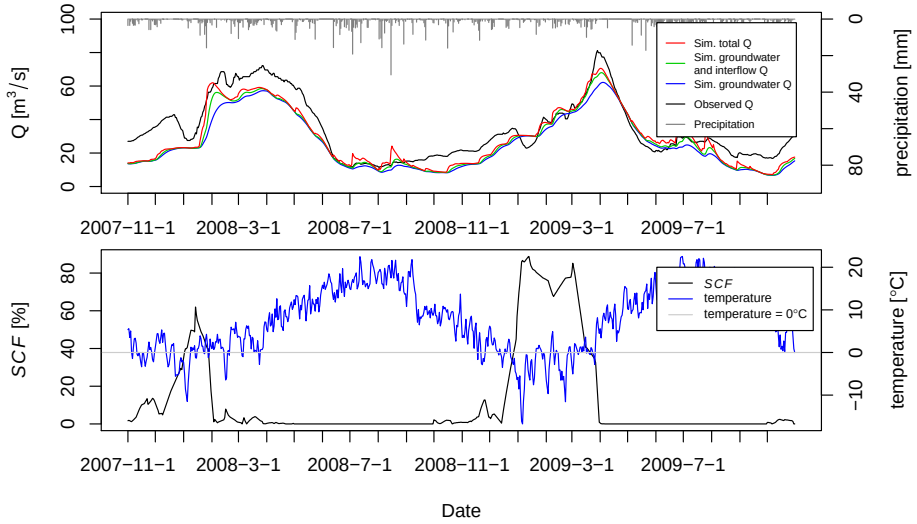

Figure 6. Observed and simulated discharge used for SA (upper panel). Also presented is WetSpa simulated groundwater and interflow discharge as well as only groundwater discharge. Catchment average temperature and SCF in the same period is presented in the lower figure.

HESSD
11, 11987–12025, 2014

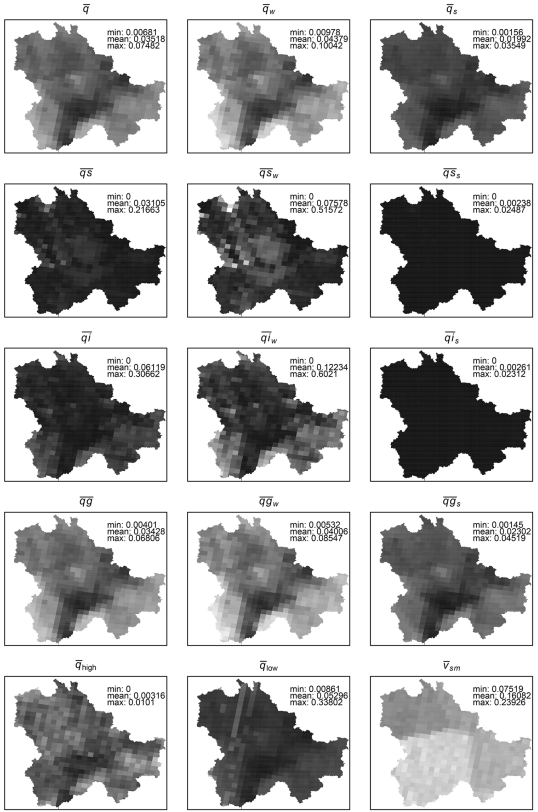

Figure 7. The SCF sensitivity maps of the Biebrza River catchment for the WetSpa model for different RF. The grey scale represents linearly stretched $s_j^{\star}$ values between minimum (black) and maximum (white) values; for the top four rows the minimum and maximum values are selected to match the data range of all maps in each row; in the lowest row each map has individual grey scale between the minimum and maximum values indicated on the plots. Explanation of the RF is presented in Table 1.

HESSD
11, 11987–12025, 2014

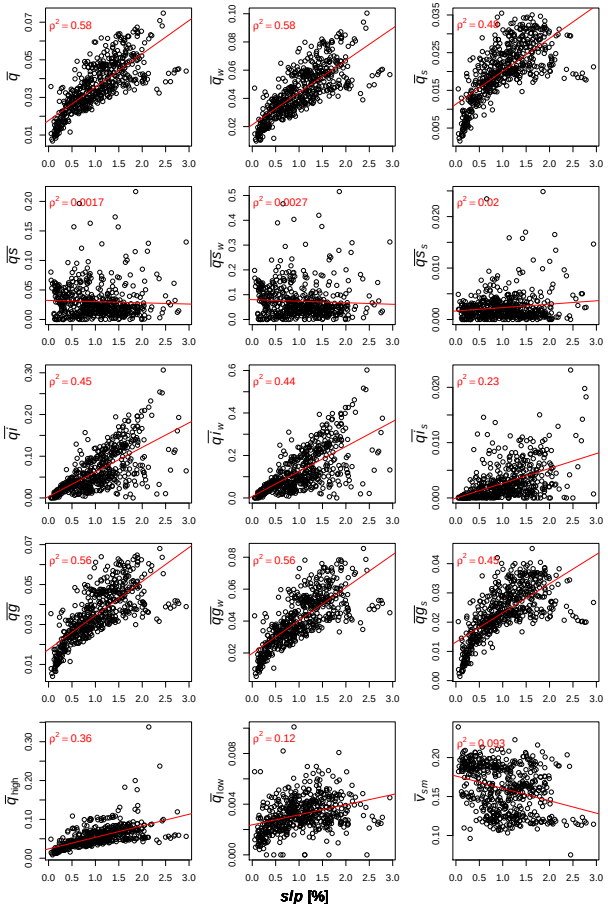

Figure 8. Relation between slp and spatial SA quantified with different RF's. Explanation of the RF is presented in Table 1.

HESSD
11, 11987–12025, 2014

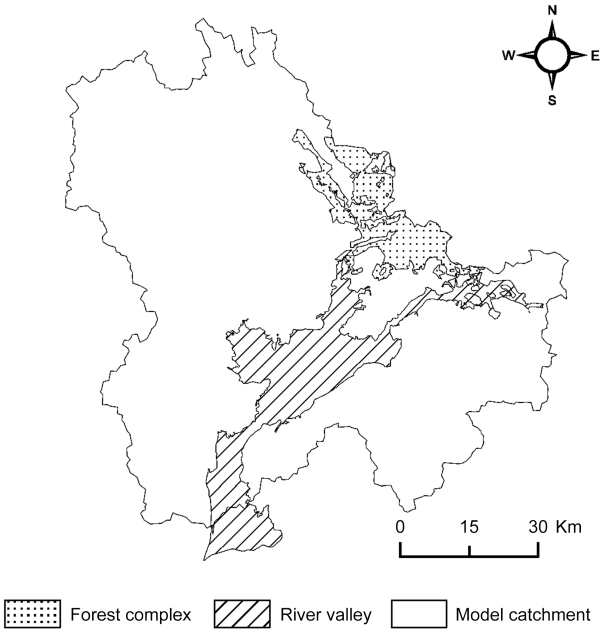

Figure 9. Major landscape features of the Biebrza River catchment. The Biebrza River valley runs NE–SW through the catchment with at the upstream part of the valley a large forest complex. Catchment area outside the river valley is upland/plateau with mineral soils.

HESSD
11, 11987–12025, 2014